



Review

# Review of Capillary Rise Experiments for Surface-Active Solutes in the Subsurface

Sebnem Boduroglu \*  and Rashid Bashir

Department of Civil Engineering, Lassonde School of Engineering, York University, Toronto, ON M3J 1P3, Canada

\* Correspondence: sebnembo@yorku.ca

**Abstract:** Surface-active solutes that exist in the subsurface either naturally (humic acid) or as a result of anthropogenic activities (alcohols, surfactants, PFAS) alter the hydraulic and geotechnical properties of the unsaturated porous media. The alteration of properties is the result of concentration-dependent surface tension, and/or density, and the contact angle effects. These effects are manifested in the form of changes in water retention and conduction and changes in the suction component of the shear strength. Differences in the spatial distribution of these solutes in the subsurface result in capillary pressure gradients causing flow perturbations. Conceptual and numerical models to understand the effects of these solutes require concentration-dependent consideration of surface tension, density, and the contact angle effects on hydraulic and geotechnical properties of porous media. Capillary rise experiments have been carried out to either quantify the effect of surface-active solutes on the height of capillary rise or to determine the concentration-dependent contact angle changes due to salinity of the pore water. This paper provides a comprehensive review of the literature on capillary rise experiments and how they can potentially be used to characterize the hydraulic and geotechnical properties of unsaturated porous media affected by surface-active solutes.

**Keywords:** vadose zone; porous media; capillarity; capillary rise experiments; capillary rise method; upward infiltration; surface-active solutes; PFAS; surfactants; contact angle

**Citation:** Boduroglu, S.; Bashir, R.

Review of Capillary Rise

Experiments for Surface-Active

Solute in the Subsurface. *Geotechnics***2022**, *2*, 706–730. <https://doi.org/10.3390/geotechnics2030034>Academic Editor: Kenneth Imo-Imo  
Israel Eshiet

Received: 26 July 2022

Accepted: 18 August 2022

Published: 20 August 2022

**Publisher's Note:** MDPI stays neutral with regard to jurisdictional claims in published maps and institutional affiliations.



**Copyright:** © 2022 by the authors. Licensee MDPI, Basel, Switzerland. This article is an open access article distributed under the terms and conditions of the Creative Commons Attribution (CC BY) license (<https://creativecommons.org/licenses/by/4.0/>).

## 1. Introduction

Capillarity at the pore scale depends on four factors: the surface tension and density of the liquid, the contact angle at the solid-liquid interface, and the pore radius. Reduction in surface tension is the fundamental effect of surface-active solutes even in low concentrations. Surface-active solutes tend to accumulate at the boundary phases and reduce the interfacial tension at the interface of two immiscible fluids. Moreover, the solid-liquid contact angle and/or soil water density might also be altered due to the presence of surface-active solutes [1,2]. Changes in soil capillarity due to surface-active solutes in the subsurface result in changes in soil water retention and conduction properties [3,4]. The presence of surface-active solutes in unsaturated flow systems can cause flow perturbations due to their concentration-dependent effects on surface tension and contact angle. It has been reported that these flow perturbations occur as a result of capillary pressure differences between regions of higher surface-active solute concentration (lower surface tension, higher pressure) and lower surface-active solute concentration (higher surface tension, lower pressure) [5,6]. Moreover, as a consequence of clean water infiltration into the vadose zone with surface-active solute contamination, a solute-dependent capillarity-induced focused flow (SCIFF) region may be observed [7,8]. In the SCIFF region, pure water is forced to move within narrow finger-patterned vertical flow pathways due to being constrained by the surfactant-induced pressure gradients in the horizontal direction [9]. Another indication of the presence of surface-active solutes in the subsurface is the reduction in the water holding capacity of the system, which results in capillary fringe depression [10].

Capillary rise occurs spontaneously where liquids rise into relatively dry hydrophilic porous media against gravity and friction forces. Similarly, capillary rise in the vadose zone

describes the upward movement of soil water driven by the pressure gradient acting across the curved air/water interface [11]. Capillary rise leads to an increase in water content, which changes the soil's strength and elastic modulus, hence the soil's stress and strain response under an external load; therefore, it can impact the stability and serviceability of structures [12]. For example, capillary rise is particularly critical to be considered when designing infrastructures in frost heaving zones [13]. Additionally, climate change causes intense and inconsistent precipitation patterns, resulting in sudden water table fluctuations and an increased number of shrink–swell cycles, which can cause surface cracks due to evaporation and desiccation. As the soil dries out, equilibrium is re-established by the movement of soil water from wetter soil towards drier soil [14].

For soils, geometric measurement of contact angle is not possible because planar surfaces for such measurements are not existent, which leads to the necessity of simplifying the complex geometric arrangement of soils into a bundle of capillary tubes [15]. The contact angle in soils is too complex to be defined by a single contact, therefore it should be defined as “a statistical distribution associated with the varied surfaces found in the medium” and must be recognized as an effective parameter for the heterogeneous porous medium under investigation [16]. Although contact angle is an essential parameter to understanding the interfaces and wettability in the subsurface, the importance of the contact angle is not sufficiently recognized in the literature [17]. Contact angle influences water retention in porous media [18] and it can also be used as an index of soil hydrophobicity [19]. Soil hydrophobicity is mainly caused by an increase in organic hydrophobic compounds derived from living or decomposing plants or microorganisms, soil temperature due to wildfires and contamination by surface-active solutes [20–22]. These factors result in changes in contact angle and therefore soils become hydrophobic. Soil hydrophobicity hinders water infiltration and causes water ponding, enhanced runoff, fingered preferential flow paths, and uneven water distribution in soil profiles [23,24]. Capillary rise experiments can be used to determine the contact angle and the wetting properties of porous media through indirect procedures to circumvent the need for direct geometric contact angle measurements. Moreover, various surface-active contaminants of geo-environmental interest and their effects on soil capillarity can be also investigated by capillary rise experiments. This paper provides a review of literature on capillary rise experiments in porous media with a focus on how these experiments are being/can be utilized to quantify the influence of surface-active solutes on vadose zone flow and transport.

## 2. Surface-Active Solutes of Geo-Environmental Interest

### 2.1. Alcohols

Solvents are used to steer chemical processes by leading to different reaction pathways in chemical synthesis [25]. Short-chain alcohols, such as 1-butanol and ethanol are commonly used as industrial solvents [25,26]. Moreover, 1-butanol and ethanol production gained more attention in recent years because they can be blended with gasoline and used for alternative fuel production [27,28]. As the overall industrial and commercial consumption of 1-butanol and ethanol increase, so does the risk of 1-butanol and ethanol spills and their contamination of the environment [26]. These high solubility alcohols cause surface tension depression in soil water which results in flow perturbations, increased drainage, and depression of capillary fringe [1]. Additionally, it has been reported that adding ethanol and butanol into gasoline interferes with natural attenuation processes and may result in more persistent hazardous aromatic hydrocarbon plumes [27].

### 2.2. Surfactants

Surface-active agents, which are commonly called surfactants, are a group of organic compounds with a special amphiphilic molecular composition. Each surfactant molecule has a hydrophilic moiety (water-liking head) and a hydrophobic moiety (water-hating tail). Surfactants are mainly classified based on the charge on their hydrophilic head (Figure 1) as nonionic (no apparent charge), anionic (negatively charged), cationic (positively charged)

or zwitterionic (both positively and negatively charged) [29]. The hydrophobic tail consists of a hydrocarbon chain, which usually contains 12 or more carbon atoms [30].

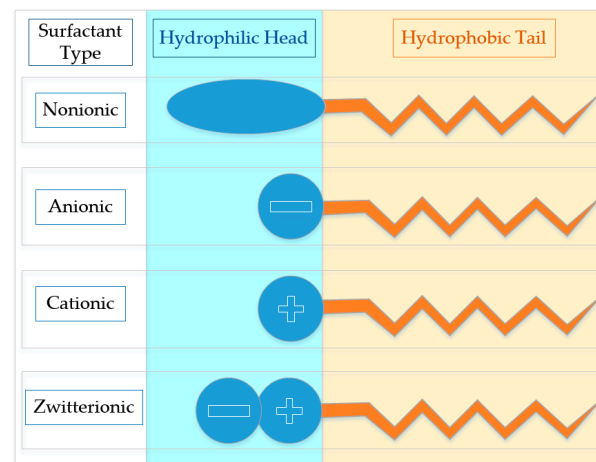


**Figure 1.** Surfactant classification according to the composition of their hydrophilic head.

Surfactants tend to accumulate at the boundary phases and reduce the surface/interfacial tension at liquid–gas interface/liquid–liquid interface of two immiscible fluids, which enhances mobilization of non-aqueous phase liquids (NAPLs) (Figure 2a). As the surfactant concentration continues to increase (Figure 2b), surfactant molecules saturate the interface and they start moving in water in the form of monomers. When the surfactant concentration reaches its critical micelle concentration (CMC), micelle formation takes place (Figure 2c), which improves the aqueous solubility of otherwise insoluble NAPLs.

Surfactants can exist in the subsurface either naturally (humic acid) or could be introduced anthropogenically. Anthropogenic activities using surfactants are mainly related to greywater reuse for irrigation purposes [21,31,32], soil/groundwater remediation techniques [33], or enhanced oil recovery purposes [34]. In arid and semi-arid climates, greywater is increasingly being used by households for irrigation purposes, commonly without proper treatment [35]. Greywater refers to wastewater from baths, sinks, washing machines, and other kitchen appliances, which represents 60–75% of domestic wastewater [36] with surfactant concentrations that can range from 0.7 to 70 mg/L [37]. Water quality standards for domestic water recycling vary between different countries and lack global standardization [36]. Additionally, deficiency of standardized greywater treatment techniques causes households to use greywater without proper treatment [38], which introduces surfactants into the subsurface. Surfactants in greywater are mainly generated from household cleaners (mainly laundry and dishwashing detergents) and personal cleansing products [39]. Surfactant consumption data from Europe [40], Canada, and the United States [41] indicate that the most widely used surfactant type is anionic surfactants, with linear alkyl benzene sulfonates (LAS) being the most popular group for both cases. The Human and Environment Risk Assessment Agency (HERA) reports that the most recent and realistic market survey on LAS consumption estimated 430,000 tons of total usage out of which 80% of the LAS (roughly 350,000 tons) was estimated to be used by households [42]. Even in cases of proper treatment, long-term irrigation with treated wastewater is reported to result in increased salt, sodium, and organic matter content in the subsurface, resulting in reduced hydraulic conductivity and water infiltration instabilities [43].

Similar to their effect on dirt and stains on dishes and clothing, surfactants are also used for contaminant removal purposes from the soil by reducing the interfacial tension between the contaminant and the groundwater and thereby enhancing the contaminant's mobility [45]. Additionally, surfactants also increase a contaminant's solubility as a result of micelle formation [46]. Although surfactant-enhanced soil washing may have many advantages for in-situ contaminant recovery, one of the downsides and main points of

concern for this technique is the introduction of surfactants into the subsurface, which can create secondary contamination [47]. Surfactant-enhanced soil washing can be carried out either ex-situ or in-situ. The contaminated soil is excavated and treated at the surface for ex-situ soil washing, whereas in-situ soil washing treats the soil in place [48]. Injecting surfactants as an in-situ soil remediation technique was incipiently used for petroleum recovery operations; later, surfactants were also used for aquifer remediation and the removal of heavy metals and radionuclides from soil [49,50].

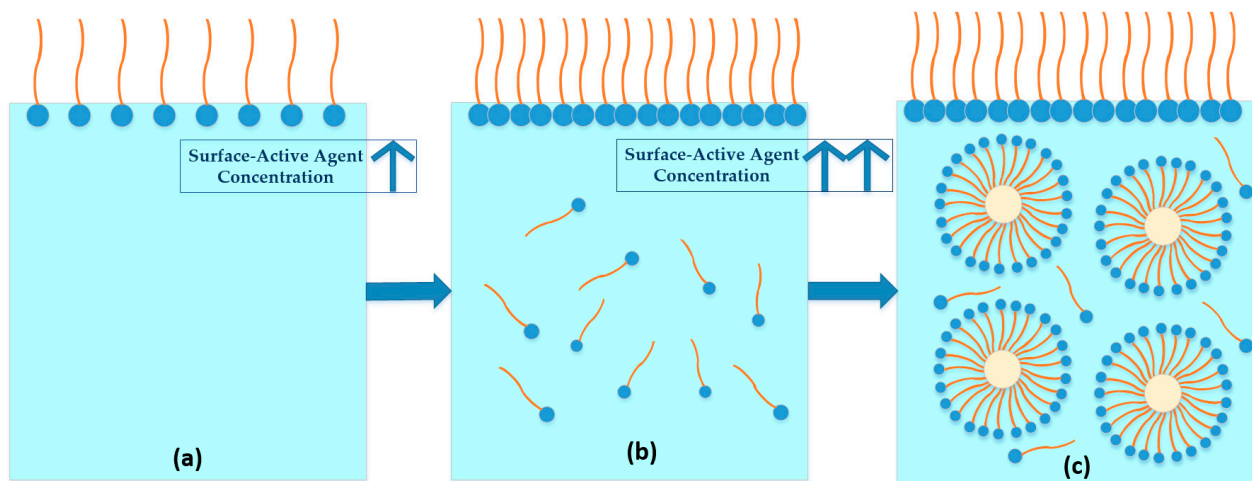


**Figure 2.** Surfactant micelle formation in water, modified from [44]. (a) Surfactants reduce the surface tension of water by adsorbing at the liquid-gas interface. (b) As the surfactant concentration continues to increase, surfactant molecules saturate the interface and they start moving in water in the form of monomers. (c) When the surfactant concentration reaches CMC, micelle formation takes place, which improves the aqueous solubility of otherwise insoluble NAPLs.

Due to climate change and increasing population, water pollution and freshwater scarcity will continue to be the most significant problems of our time [51] and the effects of surfactant accumulation in the subsurface will be more and more critical in the future [52]. Besides surfactants' adverse effects on plant health [37] and natural ecosystems [53] and their possible contribution to soil hydrophobicity [21], researchers also report changes in the mechanical properties of soil in the presence of surfactants, such as reductions in tensile strength [54]. Considering the above-mentioned points, it is striking to see that current literature on the fate of surfactants and their effects on flow and transport in the subsurface is very limited.

### 2.3. Perfluoroalkyl and Polyfluoroalkyl Substances (PFAS)

PFAS contain "one or more C atoms on which all the H substituents (present in the nonfluorinated analogues from which they are notionally derived) have been replaced by F atoms, in such a manner that they contain the perfluoroalkyl moiety  $C_nF_{2n+1}$ " [55]. PFAS are often dubbed as "forever chemicals" since they can take decades to break down because of their strong and stable C–F bonds which cause them to be extremely persistent and exceptionally resistant to degradation [56]. PFAS comprise a group of 4700 individual highly fluorinated synthetic substances which are widely used in highly diverse industrial, commercial, and military applications since 1950 [57]. Perfluorooctane sulfonic acid (PFOS) and perfluorooctanoic acid (PFOA) are the most widely studied end products of the environmental transformations of PFAS [57,58]. PFAS can be categorized into two, according to their chain length: short-chain or long-chain. The Organization for Economic Co-operation and Development (OECD) defines long-chain PFAS as "perfluoroalkyl carboxylic acids (PFCAs) with  $\geq 7$  perfluorinated carbons and perfluoroalkane sulfonic acids (PFSAs) with  $\geq 6$  perfluorinated carbons" and they have been identified

as highly persistent, bio-accumulative, and toxic [59]. Many PFAS act as surfactants due to the water- and oil-repellency of their perfluoroalkyl moiety and their high chemical and thermal stability [59]. Although long-chain PFAS have better surface-active properties, in recent years short-chain PFAS are being used as surfactants due to their lower bioaccumulation potential and less alarming environmental properties in comparison to long-chain PFAS [60]. Considering that the short-chain PFAS are extremely mobile due to their relatively low sorption properties, they cannot be removed from water using activated carbon filters compared to their long-chain homologues; the concentrations in short-chain PFAS-contaminated areas (provided that no further release occurs) will only decline with further spatial distribution [60].

Similar to surfactants, in concentrations above their CMC, PFAS form micelles by removing their hydrophobic tails from water (Figure 3A). If water becomes heavily dominated by hydrophobic compounds (e.g., fire training facilities' leachates), PFAS tend to form inverted micelles, where hydrophilic heads stay at the inner core while maintaining hydrophobic interfaces at the outer micelle surface (Figure 3B) [56].

According to the U.S. Environmental Protection Agency's (EPA) PFAS Strategic Roadmap announced in October 2021, key industries with significant documented discharges include PFAS production and processing, metal finishing, airports, pulp and paper, landfills, and textile and carpet manufacturing [61]. High water solubility (9500 mg/L at 25 °C) leads PFAS to accumulate in surface waters (especially oceans), where they are found to be stable to hydrolysis with half-lives of 41 years for PFOS and 92 years for PFOA, respectively [62]. Plants can uptake PFAS from contaminated soils [63] and PFAS are found in many livestock products, such as liver, kidney, eggs, milk, and muscle/meat [64]. For epidemiological studies, PFAS concentrations in human serum are usually used as a biomarker of exposure, and PFAS are found to adversely affect hepatic, cardiovascular, immune, and developmental systems in the human body [62]. Moreover, PFAS are recently reported to be found in follicular fluid from women experiencing infertility [65]. In June 2022, EPA announced a total of \$5 billion for fiscal years 2022–2026 in grant funding to confront PFAS pollution in drinking water [66].

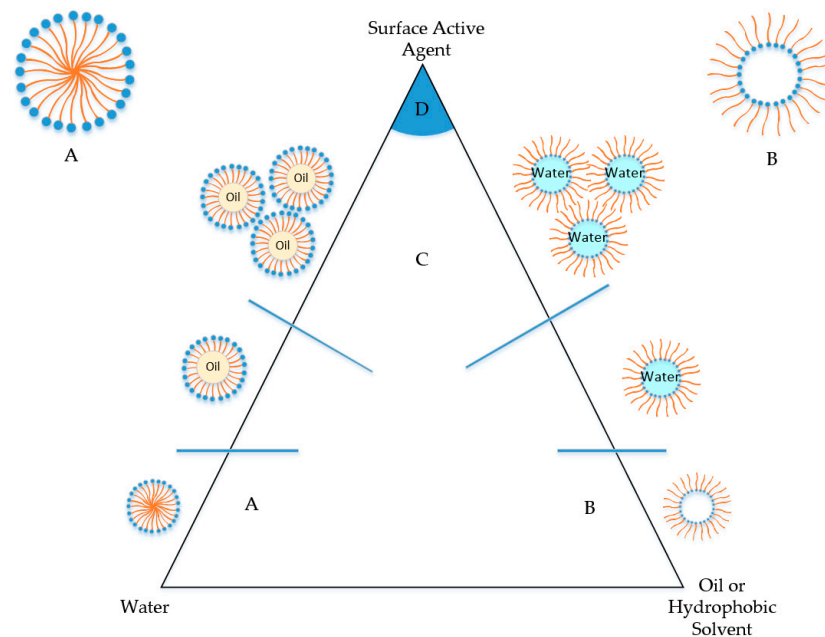


**Figure 3.** Phase diagram of an oil–water–surface-active agent microemulsion system, where shaded areas represent multiphase regions, modified from [67]. (A) Normal micelles: oil-in-water microemulsions in water (modified from [56]); (B) Reverse micelles: water-in-oil microemulsions in oil or water which is heavily dominated by hydrophobic compounds (modified from [56]); (C) concentrated microemulsion domain; and (D) liquid-crystal or gel phase.



### 3. Basic Theory of Capillarity

More than three hundred years ago, simple capillary actions such as the soaking up of water by a sponge, or the rising of wetting fluid in a capillary tube, puzzled many researchers (including Isaac Newton) since capillarity contradicted gravitation and Newtonian laws of attraction as well as Aristotelian laws of motion where matter tries to “rest” in the lowest possible position relative to the ground surface [68].

$$h = \frac{2\sigma \cos\gamma}{\rho gr} \tag{1}$$

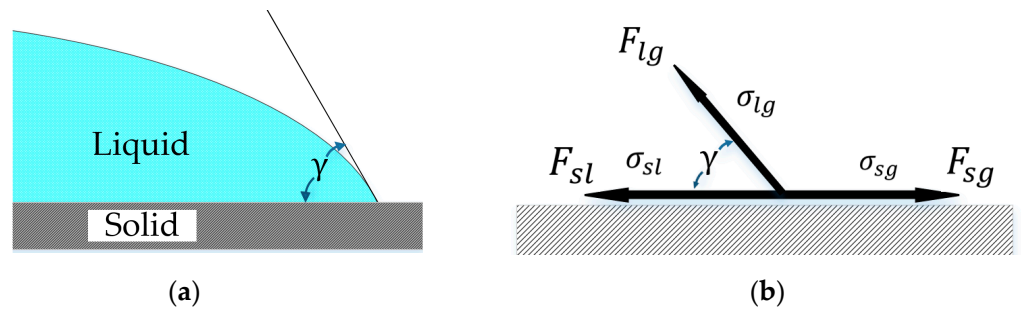
Jurin was the first researcher to solve the capillary rise in a tube and derive the liquid height ( $h$ ) from surface tension ( $\sigma$ ), contact angle ( $\gamma$ ), density of the liquid ( $\rho$ ), gravitational acceleration ( $g$ ), and tube radius ( $r$ ) (Equation (1)) [69]. In 1805, nearly 85 years after Jurin’s article, two seminal publications of capillarity research took place: Young’s essay and Laplace’s supplement to his treatise [70,71].

Wetting can be defined as the displacement of one fluid by another fluid, taking place at a solid surface (Figure 4a). From a geotechnical perspective, this may represent a simplified air–water interface in unsaturated soil zone. Since the system is at equilibrium, the balance of the forces in the horizontal direction (Figure 4b) leads to the Young–Laplace equation (Equation (2)).

$$\sigma_{lg} \cos\gamma = \sigma_{sg} - \sigma_{sl} \tag{2}$$

where  $\sigma_{lg}$  is the surface tension at liquid–gas interface,  $\gamma$  is contact angle,  $\sigma_{sg}$  is the surface tension of the solid–gas interface,  $\sigma_{sl}$  is the surface tension of the solid–liquid interface. Solving Equation (2) for the contact angle leads to Equation (3),

$$\gamma = \cos^{-1} \left( \frac{\sigma_{sg} - \sigma_{sl}}{\sigma_{lg}} \right) \tag{3}$$



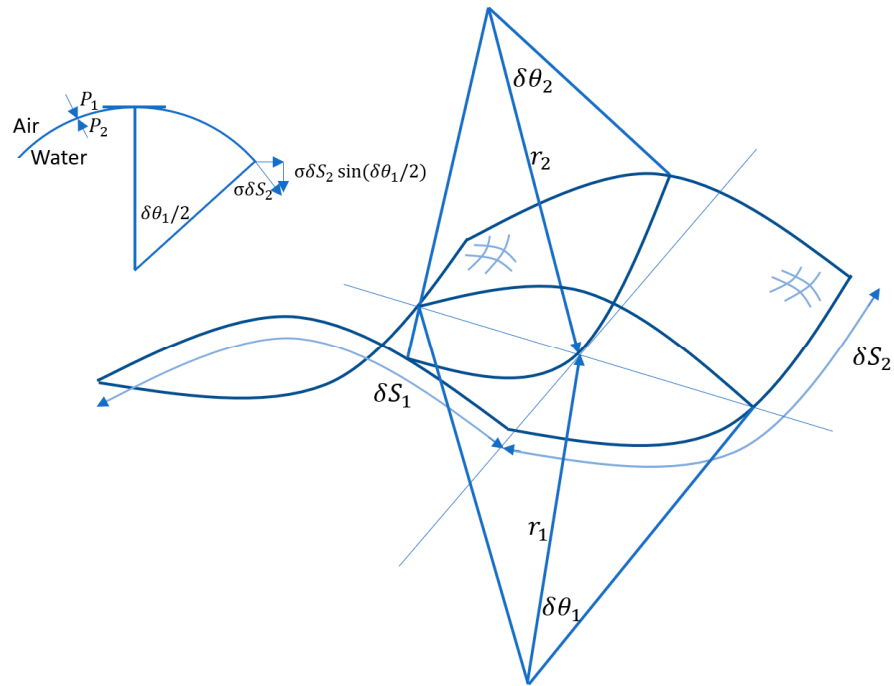
**Figure 4.** (a) Cross sectional representation of liquid/air contact with a solid; (b) horizontal balance of forces at the point of contact at equilibrium which yields to Young–Laplace equation, modified from [72].

Figure 5 is a representation of how surface tension manifests itself in a porous medium at the air–water interface [72]. Considering that the system is in equilibrium, the summation of forces in upward and downward directions should be zero. Forces acting upward ( $F_{upward}$ ) resulting from pressure ( $P_2$ ) acting on the surface area  $\delta S_1 \delta S_2$  are shown in Equation (4),

$$F_{upward} = P_2 \delta S_1 \delta S_2 + 2\sigma \delta S_1 \sin \left( \frac{\delta\theta_2}{2} \right) \tag{4}$$

Symmetrically, downward forces are given in Equation (5),

$$F_{downward} = P_2 \delta S_2 \delta S_1 + 2\sigma \delta S_2 \sin \left( \frac{\delta\theta_1}{2} \right) \tag{5}$$



**Figure 5.** An anticlastic (doubly curved) liquid surface, modified from [72].

Small angle approximation for  $\delta\theta_1$  and  $\delta\theta_2$  leads to Equation (6).

$$\sin\left(\frac{\delta\theta_1}{2}\right) \approx \frac{\delta\theta_1}{2} \approx \frac{\delta S_1}{2r_1} ; \sin\left(\frac{\delta\theta_2}{2}\right) \approx \frac{\delta\theta_2}{2} \approx \frac{\delta S_2}{2r_2} \tag{6}$$

Zero net force assumption in equilibrium results in Equation (7).

$$F_{net} = 0 = F_{upward} - F_{downward} = P_2\delta S_1\delta S_2 + 2\sigma\delta S_1\frac{\delta S_2}{2r_2} - P_2\delta S_2\delta S_1 - 2\sigma\delta S_2\frac{\delta S_1}{2r_1} \tag{7}$$

Cancellation of  $\delta S_1\delta S_2$  simplifies Equation (7) to Laplace’s equation for pressure across an anticlastic surface, provided in Equation (8).

$$P_2 - P_1 = \sigma\left(\frac{1}{r_1} - \frac{1}{r_2}\right) \tag{8}$$

Assuming a spherical surface ( $r_1 = -r_2 = R$ ), Laplace’s equation simplifies to Equation (9), which also holds true within a capillary tube of radius R.

$$\Delta P = \frac{2\sigma}{R} \tag{9}$$

The reason why the capillary action drives water to go up in tubes can be explained by thermodynamics [72]. The wetting takes place spontaneously because the interfacial energy of the air–solid interface is larger than the water–solid interface. Water coats the surface of the capillary tube simply to minimize its free energy. An equilibrium is reached when rates of changes in the release of the surface energy ( $E_s$ ) (Equation (10)) balance out the gravitational energy ( $E_G$ ) of the system (Equation (11)).

$$E_s = \int_0^h 2\pi r (\sigma_{sl} - \sigma_{sg}) dh = 2\pi r (\sigma_{sl} - \sigma_{sg}) h \tag{10}$$

$$E_G = \int_0^h \rho g \pi r^2 h dh = \frac{\rho g \pi r^2 h^2}{2} \tag{11}$$

A stable elevation is established in equilibrium which means the rate of change in height should be equal, as provided in Equation (12).

$$\rho g \pi r^2 h = -2\pi r (\sigma_{sl} - \sigma_{sg}) \tag{12}$$

Solving Equation (12) for h leads to Equation (13).

$$h = -\frac{2(\sigma_{sl} - \sigma_{sg})}{\rho g r} \tag{13}$$

Equation (13) is only true for cases of  $\sigma_{sl} - \sigma_{sg} = \sigma_{lg}$  and therefore a zero contact angle (Equation (3)), where the shape of the meniscus will be a perfect hemisphere with its radius of curvature (R) equal to the radius of the capillary tube (r). Zero contact angle case is represented as a semicircle as shown in 2D drawing in Figure 6a. On the other hand, Figure 6b shows a nonzero contact angle case in a capillary tube with same radius, where the shape of the meniscus is altered in comparison to zero contact angle case. This is due to effect of contact angle ( $\gamma$ ) on the radius of curvature (R), as represented in Figure 6c.

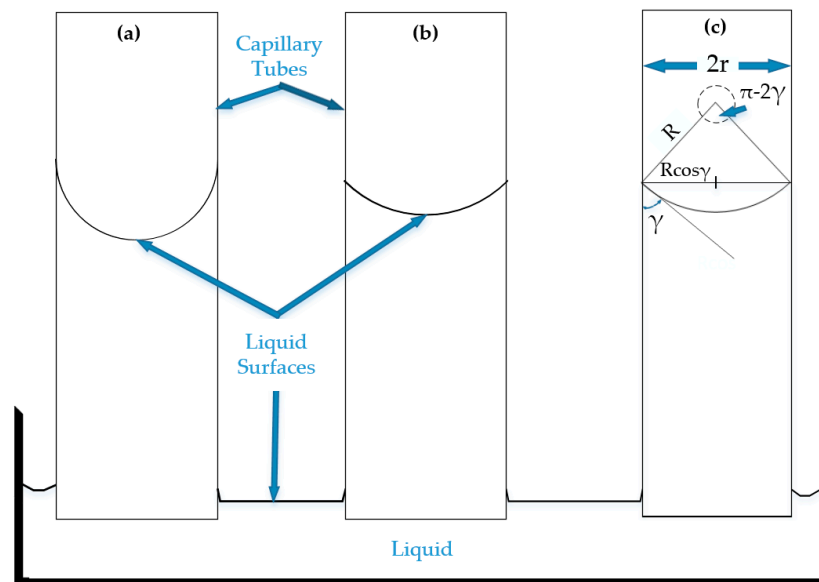


**Figure 6.** Effect of contact angle on capillary action pulling up the liquid inside the capillary tubes with the same radii. (a) Zero contact angle between the liquid and the tube; (b) nonzero contact angle between the liquid and the tube, modified from [72]; (c) geometric representation of the shape of the meniscus, radius of curvature (R) to the radius of the capillary (r) and the contact angle ( $\gamma$ ), modified from [73].

#### 4. Surface-Active Solutes’ Effects on Hydraulic Properties of Unsaturated Porous Media

##### 4.1. Concentration-Dependent Surface-Active Solutes’ Effects on Capillarity

According to Equation (1), surface tension is directly proportional to the soil water pressure head. For surface-active solutes that decrease surface tension with no discernible effect on soil water contact angle or density, the soil water pressure head can be scaled solely on the ratio of surface tension of the surface-active solute to the surface tension of pure water (Equation (14)) [10],

$$h^*(\theta, c) = h(\theta, c_0) \frac{\sigma(c)}{\sigma_0} \tag{14}$$

where  $h(\theta, c_0)$  represents the pressure head at reference concentration ( $c_0 = 0$ ) at water content  $\theta$ , whereas  $h^*(\theta, c)$  represents the solute concentration-dependent pressure head



at water content  $\theta$  at surface-active solute concentration  $c$ ;  $\sigma_o$  is the surface tension at the reference concentration ( $c_o = 0$ ), whereas  $\sigma(c)$  is the surface tension at surface-active solute concentration  $c$ . Many researchers have used this scaling relationship to quantify the effects of surface-active agents on surface tension, such as anionic sulphosuccinate, 1-tetradecanol, octanoic acid, 1-butanol and Dowfax 8390 [1,74]. For example, 7% *w/w* butanol solution depresses the surface tension of pure water from 72 mN/m ( $\sigma_o$ ) to 25.8 mN/m ( $\sigma(c)$ ), and this decrease in surface tension results in a proportional decrease in the pressure head and consecutively the air entry value (approximately to its one third) [10].

Some surface-active solutes can modify the contact angle and/or density in addition to the changes in surface tension. In order to quantify the effects of these type of surface-active solutes, the scaling relationship can be updated as Equations (15) [2] and (16), assuming that the contact angle hysteresis is minimal.

$$h^*(\theta, c) = \frac{h(\theta, c_o)}{\left(\frac{\sigma_o}{\sigma(c)}\right) \left(\frac{\cos \gamma_o}{\cos \gamma(c)}\right)} \quad (15)$$

$$h^*(\theta, c) = \frac{h(\theta, c_o)}{\left(\frac{\sigma_o}{\sigma(c)}\right) \left(\frac{\cos \gamma_o}{\cos \gamma(c)}\right) \left(\frac{\rho_o}{\rho(c)}\right)} \quad (16)$$

where  $\gamma_o$  and  $\rho_o$  are contact angle and density at the reference concentration ( $c_o = 0$ ) and  $\gamma(c)$  and  $\rho(c)$  are contact angle and density at surface-active solute concentration  $c$ .

#### 4.2. Concentration-Dependent Surface-Active Solutes' Effects on Soil Matrix and Saturated/Unsaturated Hydraulic Conductivity

Surface-active solutes have concentration-dependent effects on soil's saturated and unsaturated hydraulic conductivity depending on the physicochemical characteristics of the surface-active solutes and soil and pore water chemistry [1,75]. It is reported that surface-active solutes change hydraulic conductivity through direct physical effects, destruction of soil aggregate structure and production of fines, surfactant clay interactions, and induced secondary chemical reactions [76]. Direct physical effects can be listed as the viscosity effects, reduction or enhancement in contaminant clogging, formation of macro-emulsions, and adsorption of surfactants. Reduction in contaminant clogging is due to the removal of contaminants using surfactant-enhanced soil washing, which increases the effective pore size and thus hydraulic conductivity. On the contrary, the enhancement of contaminant clogging due to the micelle formations with increasing surfactant concentration can have the opposite effects. At the surfactant solution wetting front, macro-emulsion formation can lead to soil pore clogging, and this rapid loss of hydraulic conductivity may prevent surfactant solution from reaching the more contaminated parts of the medium. Surface-active solutes also tend to adsorb to soils with high clay content and/or a high fraction of organic carbon which can cause the clogging of effective pores of the soil and therefore lead to a reduction in hydraulic conductivity. Moreover, surface-active agents can result in the destruction of soil aggregate and the production of fines due to the lowered surface tension and the reduced ability of the soil matrix to hold the fine particles together. For initially hydrophilic soils, introducing surfactants tends to decrease the aggregate stability, whereas the exact opposite is observed for initially hydrophobic soils. Although more speculative than conclusive, Tumeo's survey underlines the importance of quantifying the effect of surfactants on hydraulic conductivity as well as the element of uncertainty in the quantification of these changes [1,76].

Smith and Gillham (1999) reported that the unsaturated hydraulic conductivity function could be scaled using the ratio of kinematic viscosity of the surface-active solution to the surface tension of pure water (Equation (17)) [10].

$$K(\theta, c) = \frac{v_o}{v(c)} K(\theta, c_o) \quad (17)$$

where  $K(\theta, c_o)$  is the unsaturated hydraulic conductivity at water content  $\theta$  at the reference concentration ( $c_o = 0$ ),  $v_o$  is the kinematic viscosity at the reference concentration ( $c_o = 0$ ),  $v(c)$  is the kinematic viscosity of the surface-active solution at a concentration of  $c$ , and  $K(\theta, c)$  is the scaled hydraulic conductivity of the surface-active solution at a concentration of  $c$ .

#### 4.3. Concentration-Dependent Surface-Active Solutes' Effects on Hydraulic Hysteresis

The soil–water characteristic curve (SWCC) defines the functional relationship between the water content and the soil water pressure head and therefore plays a fundamental role in the analysis of groundwater flow in unsaturated soils. The SWCC is hysteretic since the water content at a given soil water pressure head value for the wetting curve is less than that for a drying curve (i.e., soil can have different water contents at the same soil water pressure head value depending on its wetting–drying history) [77,78]. This behavior is believed to be caused by [79]: (a) irregularities in the cross-sections of the void passages, also known as the Haines' (1930) “ink-bottle” effect [80], (b) differences between the advancing and receding soil–air interface menisci (i.e., contact angle hysteresis), (c) the volume change of entrapped air at different pressure values, (d) thixotropic regain or aging due to the wetting–drying history of the soil.

Due to the experimental complexity of hysteretic SWCC measurements and the difficulty of incorporating and calibrating the hysteretic effects in numerical models [81], the SWCC is often assumed to be non-hysteretic for purposes of analysis of water and solute movement in the unsaturated zone [82]. However, neglecting the SWCC hysteresis may only be justifiable under monotonic wetting or monotonic drying conditions (e.g., during infiltration, evaporation, or gravity drainage with steady-state boundary conditions), which disregards the periodic changes in irrigation flux or evaporation rate [83,84]. However, transient sequences such as cyclic wetting and drying events (i.e., intermittent precipitation and evaporation) are quite common in the real-world scenarios of natural and irrigated environments, where some portions of the soil may be wetting whereas others may be drying [78].

Moreover, the presence of surface-active solutes in unsaturated systems adds another unique hysteretic dimension to consider in addition to the intermittent boundary conditions. Surface-active solutes lead to concentration-dependent changes in soil water pressure head. The capillary pressure differences between surface-active solute-free and surface-active solute-contaminated regions can lead to unsaturated flow, even at similar moisture contents [83]. In fact, this flow occurs from the surface-active solute-contaminated regions where surface tension is lower and capillary pressure is higher, and towards clean/cleaner regions where surface tension is higher and capillary pressure is lower. Literature defines this tendency to flow as surface-active solute-induced unsaturated flow [1]. This transient surface-active solute-induced change in moisture content results in a sequence of wetting, drainage, and re-wetting events to take place under monotonic boundary conditions [7]. In other words, the advance of surface-active solutes in unsaturated soil zone results in moisture content reversals (i.e., hysteresis) that would not be normally seen under monotonic flow conditions.

Considering the above-mentioned points, Figure 7 summarizes the general effects of surface-active solutes on flow and transport in unsaturated soil zone.

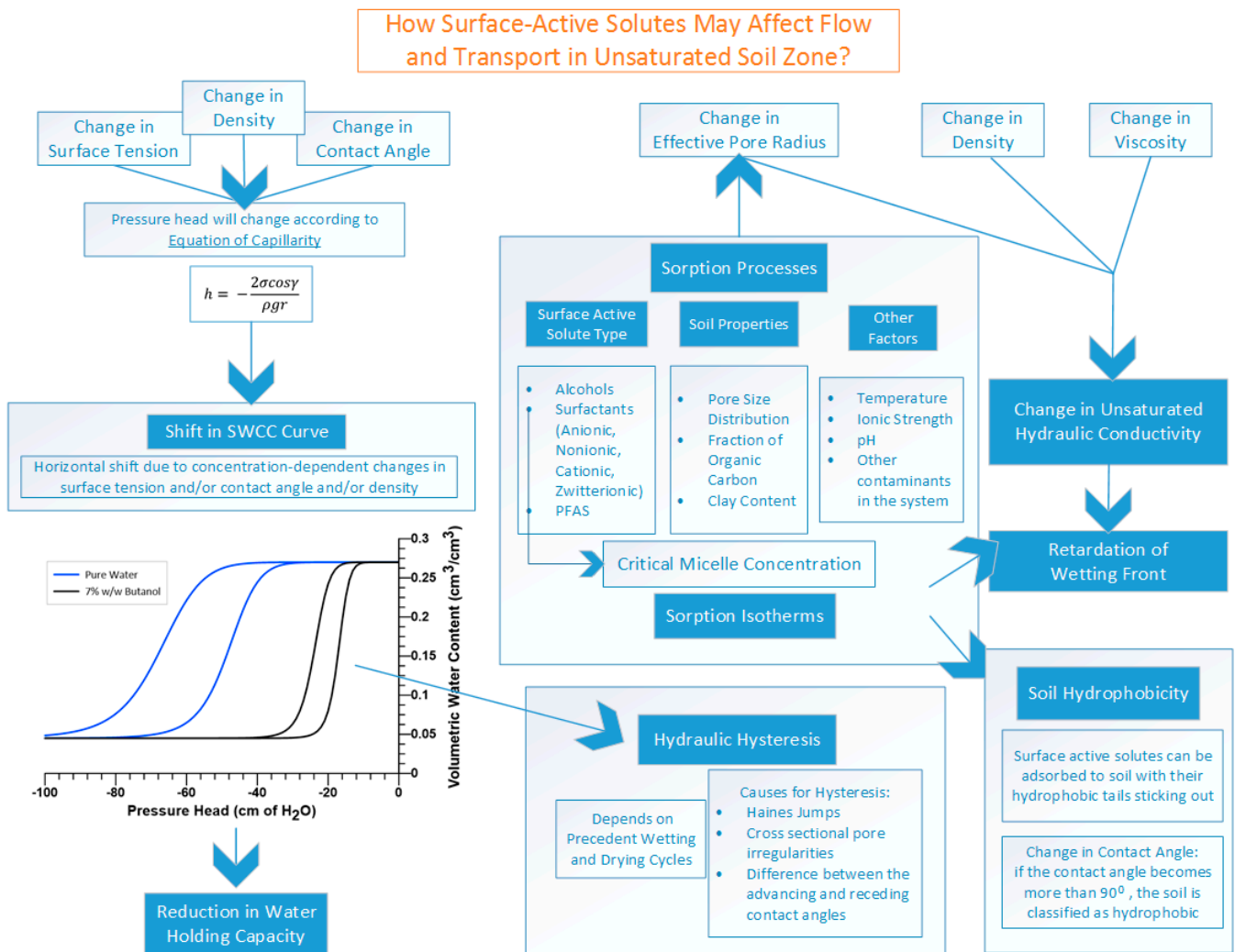


**Figure 7.** Summary of surface-active solutes’ effects on flow and transport in the unsaturated soil zone: A schematic representation.

### 5. Determination of Contact Angle in Soils

Contact angle in soils, which defines the contact on the liquid–solid interface as well as wettability properties, is an essential parameter to understanding vadose zone processes. Contact angle in soils is much more complex to be defined only by the micro-scale contact angle measured based on the idealized conceptual model of the three-phase contact point (Figure 4) [85]. Geometric measurement of the contact angle is not possible for soils because soils do not provide planar surfaces for such measurements, therefore the complex geometric arrangement of soils should be simplified into a bundle of capillary tubes using Equation (1), where *r* is the effective pore radius for the soil of interest. By this simplification, the net result of these complex processes can be represented into a single effective contact angle value averaged on a representative elementary volume containing thousands of soil grains. This is termed “effective Darcy-scale contact angle” in literature [85]. Equation (1) suggests that in cases of contact angle being equal to or greater than 90°, water will not spontaneously enter the soil [15].

Contact angle and the wetting properties of porous materials can be quantified by capillary rise experiments. Figure 8 shows a schematic representation of a capillary rise experimental setup, with a capillary tube filtered at the bottom, packed with porous medium, whose pores can be assumed to be a bundle of capillaries with an identical effective radius. The effective radius for the porous medium can be determined by completely wetting the

porous medium with a reference fluid of a known surface tension such as ethanol [86], n-hexane [85], pentane [17], or n-dodecane [87] which are assumed to have perfect wetting properties (zero contact angle).

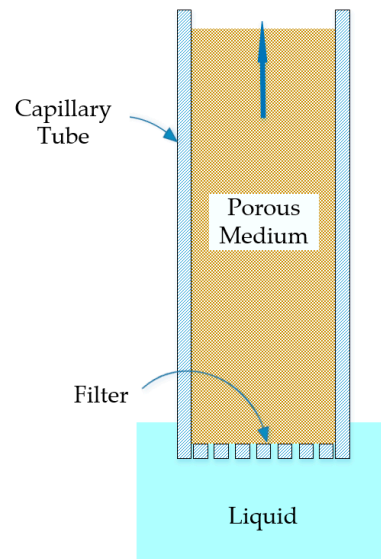


**Figure 8.** Schematic representation of “capillary rise method”, modified from [88].

Contact angle can be calculated by either measuring the rate of rise of imbibing solution or determining the pressure that should be applied to prevent the wetting fluid from entering the capillary tube [88]. This backpressure is equal to capillary pressure calculated by using the equation of capillarity (Equation (18)).

$$\Delta P_{ref} = \frac{2\sigma_{ref}}{r} \quad (18)$$

where  $\Delta P_{ref}$  and  $\sigma_{ref}$  are the backpressure and surface tension for the reference fluid, respectively, and  $r$  is the effective pore radius for the porous medium of interest. Now using the liquid under investigation in Equation (19),

$$\Delta P_L = \frac{2\sigma_L \cos\gamma_L}{r} \quad (19)$$

where  $\Delta P_L$  and  $\sigma_L$  is the backpressure and the surface tension for the liquid under investigation, respectively. Comparing  $\Delta P_{ref}$  and  $\Delta P_L$  and eliminating  $r$  leads to Equation (20), which can be directly used to calculate contact angle.

$$\cos\gamma_L = \frac{\Delta P_L}{\Delta P_{ref}} \frac{\sigma_{ref}}{\sigma_L} \quad (20)$$

## 6. Experimental Studies of Capillary Rise

### 6.1. Estimations of Capillary Rise Height

The extent to which water can rise above the ground water table is an important geotechnical/geoenvironmental design consideration for many reasons. Capillary rise can influence the depth of frozen soil and impact settlement characteristics of structures, whereas erosive ions in capillary water can damage construction materials [89]. Moreover, capillary rise could impact landfill leachate generation and movement in the subsurface [90].

There are three fundamental physical characteristics of capillary rise of primary practical concern: (i) maximum height of capillary rise, (ii) fluid storage capacity of capillary rise, and (iii) rate of capillary rise [11,89]. Figure 9 shows the conceptual model of capillary rise and the relationship between water content and soil water pressure head in the

subsurface. There are three distinct zones: (I) a saturated soil zone below the groundwater table, (II) a quasi-saturated soil zone [91] (with its larger voids accommodating occasional air bubbles [92]) above the groundwater table but below the air-entry value ( $h_a$ ) which is determined by the soil pore size [92] and pore water properties (surface tension, contact angle and density), and (III), an unsaturated soil zone above  $h_a$  with a series of connected or disconnected capillary fingers with an ultimate height of  $h_c$  [11]. However, the rate of the capillary rise depends on the highly nonlinear relationship between hydraulic conductivity and the suction head [89]. Water content decreases as the soil becomes more unsaturated, and so does its unsaturated hydraulic conductivity; in fact, hydraulic conductivity can be reduced from its value at saturation by 5–7 orders of magnitude [11]. Therefore, as the height of capillary fingers reaches  $h_c$ , the reduction in unsaturated hydraulic conductivity as well as the reduction in the driving force ( $h_c - z$ ) leads to a significant decrease in the rate of capillary rise [11,89].

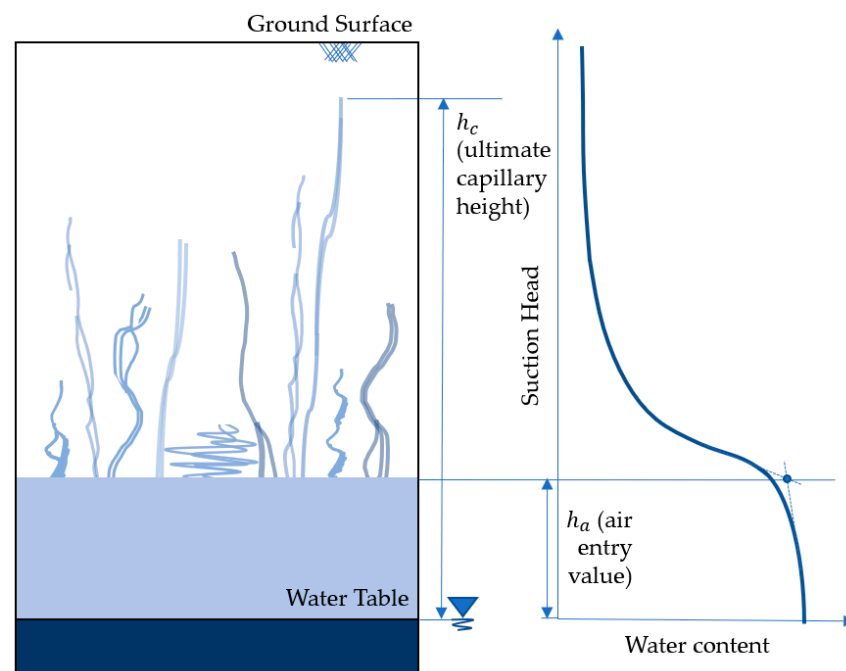


Figure 9. Conceptual model of capillary rise, and the associated water content versus suction head relationship, modified from [11].

Based on the capillary rise experiments conducted by researchers, Table 1 lists the empirical relationships in literature to estimate maximum capillary rise height.

Table 1. Empirical relationships in literature for maximum capillary rise height estimations.

Reference	Relationship (*)	Details
Lane et al. (1946) [93] Peck et al. (1974) [94]	$h_c(mm) = -990 \ln D_{10} - 1540$ $h_c(mm) = \frac{C}{eD_{10}}$	$0.006 \text{ mm} < D_{10} < 0.2 \text{ mm}$ (**) $10 \text{ mm}^2 < C < 50 \text{ mm}^2$ (***)
Kumar and Malik (1990) [95]	$h_c = h_a + 134.84 - 5.16\sqrt{r}$	$h_c$ (cm), $h_a$ (cm) and $r$ (effective pore radius in micrometers). $r = \sqrt{\frac{8\eta k_s}{\rho_w g}}$ (****)
Liu et al. (2014) [89]	$h_c = \frac{\sigma n}{\sqrt{2\eta\rho_w g k_s}} \cos\gamma + (1 - n)h_a$	$\sigma$ (surface tension), $n$ (porosity), $\gamma$ (advancing contact angle), $k_s$ (saturated hydraulic conductivity)

(\*)  $h_c$  is the ultimate capillary height,  $h_a$  is the air entry value. (\*\*)  $D_{10}$  is effective grain size corresponding to the diameter which 10% of the grains are passing in the grain size distribution curve. (\*\*\*)  $e$  is the void ratio and the constant  $C$  depends on surface impurities and grain shape. (\*\*\*\*)  $\eta$  (dynamic viscosity),  $k_s$  (saturated hydraulic conductivity),  $g$  (gravitational acceleration),  $\rho_w$  (density of water).

## 6.2. Estimation of Contact Angle

### 6.2.1. Static Capillary Rise Experiments

Methodology for static capillary rise experiments was outlined by Letey et al. in 1962 [96]. In their experiments, the data for the position of the wetting front and the volume of the solution that rose into the experimental column were collected. Equilibrium was assumed to be reached 24 h after the commencement of the imbibition event. A reference fluid (ethanol) was used to find the effective pore radius of the media ( $r$ ) using Equation (21).

$$r = \frac{2\sigma_{ref}\cos\gamma_{ref}}{\rho_{ref}gh_{ref}} \quad (21)$$

where  $ref$  denotes the reference fluid (with an assumed contact angle of zero). Since  $r$  is a geometric constant for the porous medium (packed to the same porosity), the contact angle can now be calculated using Equation (22) for the liquid under investigation as the imbibing solution.

$$\gamma_L = \cos^{-1}\left(\frac{r\rho_Lgh_L}{2\sigma_L}\right) \quad (22)$$

where  $L$  denotes the liquid under investigation.

### 6.2.2. Dynamic Capillary Rise Experiments

Static contact angles can only be measured when the system is in equilibrium or the liquid movement is sufficiently slow [97]. However, in capillary systems, liquid flow is usually fast, therefore dynamic contact angles become apparent [97]. Researchers emphasize that in the case of a moving wetting line, the contact angle should be considered dynamic [97,98]. Dynamic contact angle measurements refer to the measurements of contact angle during movement and these measurements are significantly different than their static values [98,99]. Dynamic contact angle exhibits a different value while the wetting line is advancing ( $\gamma_a$ ) or receding ( $\gamma_r$ ), which is also known as the raindrop effect (Figure 10).  $\gamma_a$  is usually significantly higher than  $\gamma_r$  and the difference between them is termed contact angle hysteresis [88].

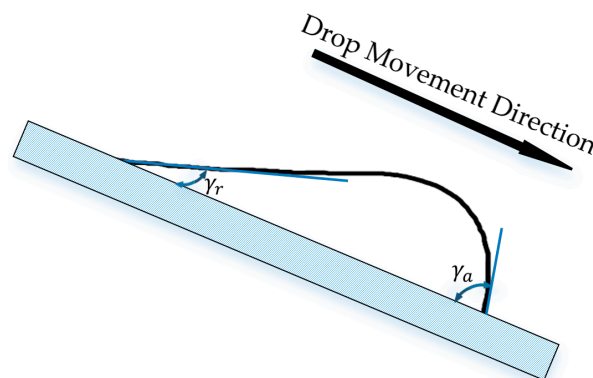


**Figure 10.** Contact angle hysteresis between advancing and receding contact angles (i.e., the raindrop effect), modified from [72].

Figure 10 shows that the plate (the medium) retains water more vigorously than it absorbs water, which can also be used to explain the relevance of contact angle hysteresis to hydraulic hysteresis [72]. Hysteretic behavior of wetting and drainage events in soils might also affect the contact angle of the system. Figure 11 illustrates Haines jumps [80] in a porous medium with identical pores connected with identical necks on the main wetting and main drainage curves of SWCC.



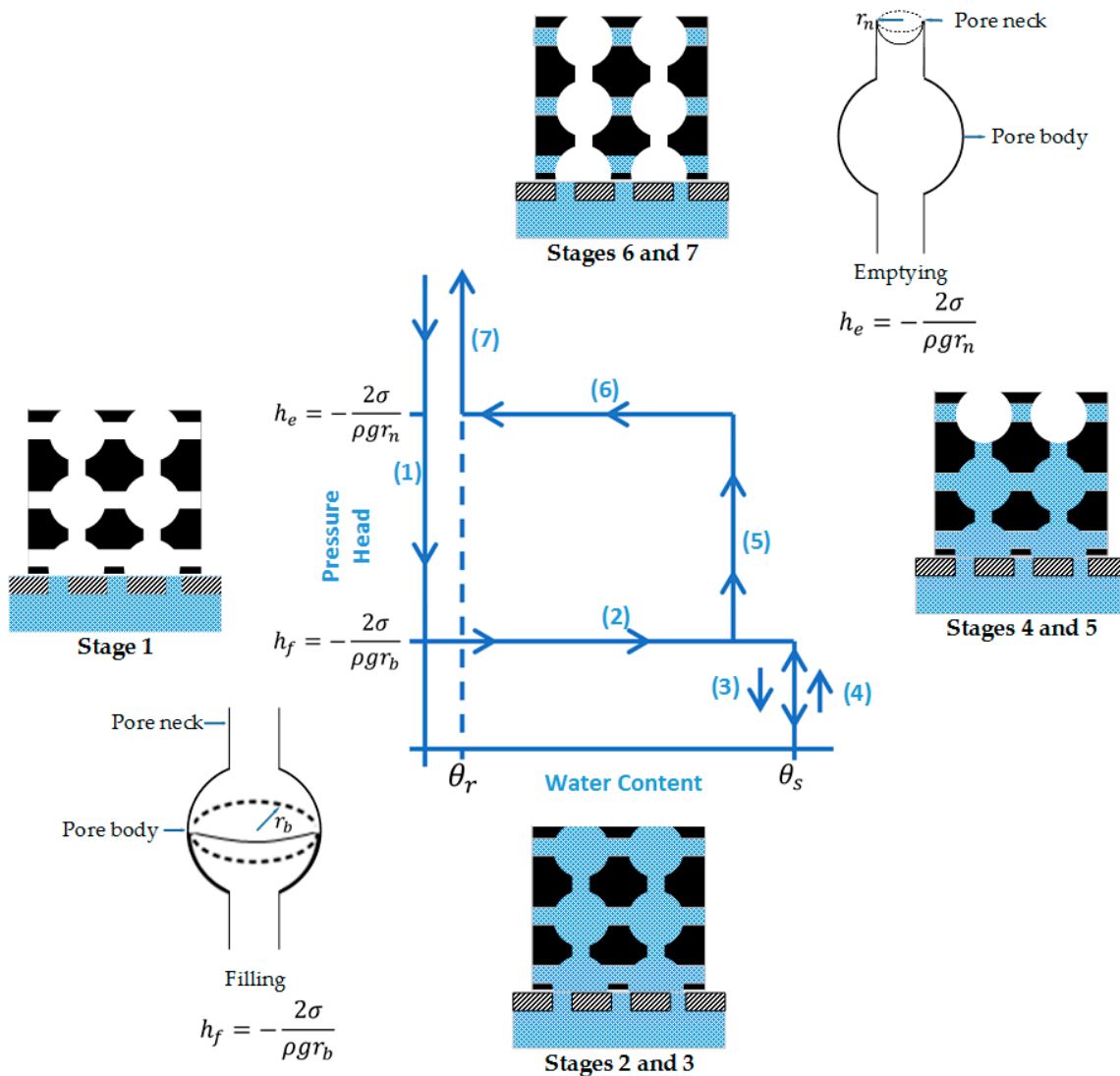


Figure 11. General understanding of “Haines jump” cycle, modified from [72].

Stages 1 to 3 illustrate a wetting event, whereas stages 4 to 7 illustrate a drainage event. Water content remains zero until the pressure head reaches  $-2\sigma/\rho g r_b$ , which is the value to sufficiently fill the largest pores in the medium (Stage 1), but then the wetting event takes place suddenly (Stage 2) until the maximum saturation is reached (Stage 3). Similarly, the drainage event does not start until the pressure is sufficient to pull the water out of the pore bodies,  $-2\sigma/\rho g r_b$  (Stage 4), however only a small portion of drainage takes place between  $-2\sigma/\rho g r_b$  to  $-2\sigma/\rho g r_n$  (Stage 5). Although most of the water can be taken out of the system under the pressure head of  $-2\sigma/\rho g r_n$  (Phase 6), the soil cannot be drained completely since some residual water remains in place and cannot be removed (Phase 7). This is due to the strong chemical bonds between water and the charged surfaces of soil grains and the formation of isolated donut shape pockets of water, also known as pendulars [72]. Therefore, the water content of the porous medium for any given pressure depends on the wetting history of the pore due to the hysteretic behavior of wetting and drainage events [83]. Additionally, instead of being steady, gradual, and continuous, the wetting event in porous media is highly nonlinear and abrupt with long pauses and sudden jumps.

A dynamic method for contact angle measurements was derived [73] based on the Washburn theory [100], which indicates that when the porous medium is brought into

contact with a liquid, the imbibition will be governed by capillary action only (ignoring gravity) (Equation (23))

$$t = Am_L^2 \tag{23}$$

where  $t$  is the time after the contact,  $m_L^2$  represents the squared mass of liquid imbibed which is measured with time and  $A$  is a constant which is dependent on the properties of the liquid and the porous medium under investigation (Equation (24)).

$$A = \frac{\mu}{c\rho^2\sigma\cos\gamma} \tag{24}$$

where  $\mu$  is the dynamic viscosity of the liquid, and  $c$  is a material constant. By combining Equations (23) and (24) and solving for contact angle leads to Equation (25).

$$\gamma = \cos^{-1}\left(\frac{m_L^2}{t} \frac{\mu}{\rho^2\sigma c}\right) \tag{25}$$

Since  $\rho$ ,  $\mu$ , and  $\sigma$  can be measured, a reference liquid such as ethanol can be again used as in the static method to calculate the porous medium specific  $c$ .

The Green and Ampt [101] conceptual model (Figure 12) is a good representation of the infiltration models of dry sandy soils experiencing sharp wetting fronts [72].

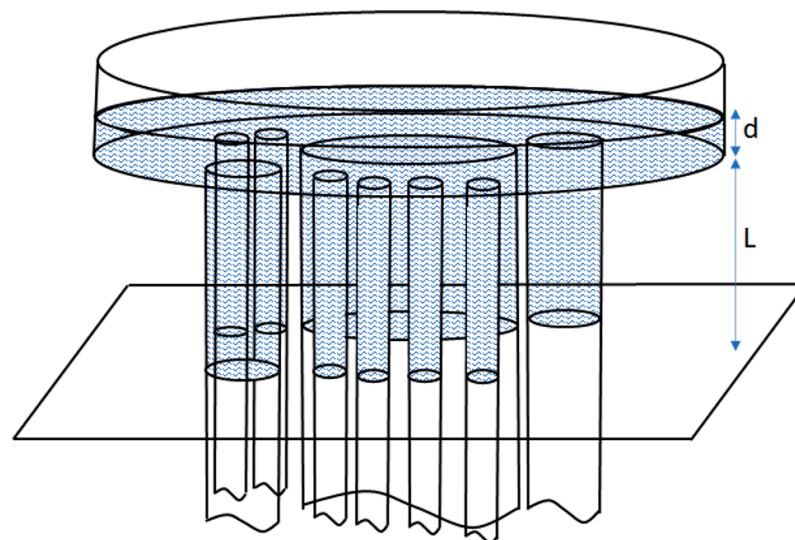


**Figure 12.** Conceptual model for Green and Ampt vertical infiltration, where  $d$  is the ponding depth, water is advanced to a depth  $L$  with the assumption of considering the porous medium with a set of parallel capillary tubes of different diameters, modified from [72].

Darcy’s law is given in Equation (26),

$$q = -K_s\left(\frac{H}{L}\right) \tag{26}$$

where  $H$  is head loss across the system and  $L$  is the distance travelled. The soil is going from dry to being fully saturated (soil’s water content at its saturation is  $n$ , which is its porosity), therefore relating the flux to the position of the sharp wetting front (Figure 12) leads to Equation (27),

$$q = \frac{d}{dt}nL \tag{27}$$

Combining Equations (26) and (27) leads to Equation (28).

$$\frac{d}{dt}nL = K_s \left[ \frac{h_f + d + L}{L} \right] \tag{28}$$

where,  $h_f$  is the potential at the wetting front,  $d$  is the depth of ponding and  $L$  is the distance traveled (could be also defined as the depth of infiltration), as illustrated in Figure 12. Equation (28) could also be used for upward imbibition by changing the sign convention, renaming  $L$  (distance traveled) as  $h$  (height of the capillary rise), and excluding ponding (since it is not relevant for capillary rise experiments), which leads to Equation (29) [102],

$$\frac{dh}{dt} = \frac{K_s}{n} \left[ \frac{h_f - h}{h} \right] \tag{29}$$

Considering that the Green and Ampt model assumes a “sharp” (fully saturated) wetting front for upward imbibition in sandy soils, Weisbrod et al. (2009) pointed out the need to use a modified version of the Green and Ampt theory, because the wetting front is actually not fully saturated and therefore actual hydraulic conductivity at the wetting front during imbibition, is indeed lower than its saturated hydraulic conductivity. The Brooks and Corey (1964) equation [103] can be used to calculate the unsaturated hydraulic conductivity (Equation (30)),

$$K_{FS} = K_S \left( \frac{\theta_{FS} - \theta_r}{n - \theta_r} \right)^{\frac{2}{\lambda} + 3} \tag{30}$$

where  $K_{FS}$  is the unsaturated hydraulic conductivity at the wetting front,  $K_S$  is the saturated hydraulic conductivity,  $\theta_{FS}$  is the volumetric water content at  $K_{FS}$ ,  $\theta_r$  is the residual water content,  $n$  is the porosity, and  $\lambda$  is a dimensionless shape factor.

Replacing  $K_S$  and  $n$  with  $K_{FS}$  and  $\theta_{FS}$  and rearranging Equation (30) leads to Equation (31),

$$dt = \frac{\theta_{FS}}{K_{FS}} \left( \frac{h}{h_f - h} \right) dh \tag{31}$$

Integrating and rearranging Equation (31) leads to Equation (32),

$$t = \frac{\theta_{FS}}{K_{FS}} \left\{ -h - h_f \left[ \ln \left( \frac{h_f - h}{h_f} \right) \right] \right\} + t_0 \tag{32}$$

where  $t$  is the predicted time and  $t_0$  is the integration constant.

Capillary rise theory outlined by Liu et al. (2014) considers four types of forces in the governing equation, which are surface tension, inertial force, viscous force, and gravity [17] (Equation (33))

$$\text{Surface Tension} - \text{Inertial Force} - \text{Viscous Force} - \text{Gravity} = 0 \tag{33}$$

Open form version of Equation (33) can be written as Equation (34) (a modified version of the Lucas–Washburn equation [17]) in the case of one-dimensional flow only when neglecting friction and inertia effect caused by displaced air, neglecting inertia and entry effect in the liquid reservoir, and assuming Hagen–Poiseuille law holds true for the viscous pressure loss inside the capillary tube [17].

$$2\pi r\sigma \cos(\gamma) - \rho\pi r^2 \frac{\partial}{\partial t} \left[ h(t) \frac{\partial h(t)}{\partial t} \right] - 8\pi\eta h(t) \frac{\partial h(t)}{\partial t} - \rho\pi r^2 g h(t) = 0 \tag{34}$$

where  $r$  is the radius of the capillary tube,  $t$  is time,  $h(t)$  is the height of capillary rise at that time. A simplified version of Equation (34) is provided in Equation (35),

$$B - A(hh')' - Chh' - Dh = 0 \quad (35)$$

where  $A = \rho\pi r^2$ ,  $B = 2\pi r\sigma \cos(\gamma)$ ,  $C = 8\pi\eta$ , and  $D = \rho\pi r^2 g$ .

Liu et al. (2014) investigated the performance of Equation (34) by neglecting different forces: without gravity and inertia (Method 1), without gravity (Method 2), and without inertia (Method 3) while incorporating the effects of tortuosity in each method. They note that Method 3 provides the best fit for their experimental results. Another important observation drawn from their work is the relationship between the contact angle and aggregate size, which is found to be dependent on organic matter content (for soils) and roughness (for silica sand) [17].

### 6.3. Capillary Rise Experiments for Surface-Active Solutes

There are very few studies available in literature which utilize capillary rise experiments to investigate the effects of surface-active solutes on capillarity.

Wiel-Shafran et al. (2005, 2006) studied the effects of surfactant accumulation due to irrigation with greywater by conducting capillary rise experiments using water, artificially prepared laundry solution, and pure surfactant solutions [37,104]. Preparation of laundry solution was performed by mixing known amounts of a commercial laundry detergent powder with tap water and measuring the anionic surfactant concentration the by methylene blue active substances (MBAS) method. Methylene blue is a cationic dye, which is insoluble in organic liquids but becomes soluble upon interaction with an anionic surfactant. The MBAS method measures surfactant concentration via spectrophotometric analysis by considering methylene blue absorbed in the organic liquid layer [105]. On the other hand, LABS-100 (linear dodecyl benzene, anionic) and Imbentin-UMG/070 (ethoxylated alcohol, nonionic) were used as pure surfactants. Authors use Equation (36) proposed by Malik et al. (1981) [106],

$$\frac{dh}{dt} = \frac{2\sigma r \cos\alpha}{G\mu} \frac{1}{h} - \frac{\rho g r^2}{G\mu} \quad (36)$$

where  $dh/dt$  is the rate of movement of the wetting front with respect to time (m/s),  $r$  is the equivalent pore radius (m),  $\mu$  is the solution's viscosity (Pas),  $G$  is the shape factor (8 for circular capillary),  $\sigma$  is surface tension (N/m),  $\rho$  is the density of the imbibing solution ( $\text{kg}/\text{m}^3$ ), and  $g$  is the gravitational acceleration ( $\text{m}/\text{s}^2$ ). Wiel-Shafran et al. note that based on the analysis of their experimental data  $dh/dt$  and the reciprocal of  $h$  ( $1/h$ ) were found to be linear. This slope of this linear relationship is Malik et al.'s (1981)  $\lambda$  (penetration coefficient) (Equation (37)), which can be defined as "advance visible wetting front in dry soil per square root of time under unit hydraulic head" and the intercept is the effective hydraulic conductivity [104,106].

$$\lambda = \sqrt{\frac{4\sigma \cos\alpha}{\mu} \cdot \frac{r}{G}} \quad (37)$$

Ishiguro and Fujii (2008) use capillary rise experiments to evaluate the effects of an anionic surfactant (sodium dodecyl sulfate—SDS) on upward infiltration in porous media with highly contrasting wettability [86]. Capillary rise experiments were conducted with imbibing SDS solutions at different concentrations into five different porous media with differing wettability properties: glass beads and sand classified as hydrophilic media and leaf mold, peat moss, and polyethylene particles classified as hydrophobic media. Ishiguro and Fujii's (2008) proposed upward infiltration theory and method of contact angle estimation is similar to Weisbrod et al. (2009) [85]. The authors introduce a simplified

Green–Ampt type upward infiltration theory under saturated conditions using Darcy’s law and the Washburn equation (Equation (38)).

$$\frac{d}{dt}nL = K_s \left[ \frac{L + h - x}{x} \right] \quad (38)$$

where  $n$  is porosity,  $L$  is the depth of the bottom of the column from the water surface,  $h$  is the height of capillary rise, and  $x$  is the distance of the infiltration front from the inflow boundary of the column. Authors note that  $h$  can be taken as a constant if the soil is assumed to be saturated under an infiltration front (sharp wetting front) during an infiltration event. Considering constants  $h$ ,  $K_s$ , and  $n$  and integrating the equation leads to Equation (39),

$$t = \frac{n}{K_s} [-x - (h + L) \log|-x + (h + L)| + (h + L) \log(h + L)] \quad (39)$$

Average pore water velocity in a cylindrical tube ( $v$ ) can be defined by the Hagen–Poiseuille equation (Equation (40)),

$$v = \frac{\rho g r^2}{8\mu} \left( \frac{\Delta H}{x} \right) \quad (40)$$

Substituting  $v$  into Darcy’s law leads to Equation (41),

$$K_s = \frac{n \rho g r^2}{8\mu} \quad (41)$$

Assuming  $L = 0$  and combining Equations (39) and (41) leads to a newly derived upward infiltration equation which is physically equivalent to the Washburn equation (Equation (42)) [86,107].

$$\frac{\rho g r^2}{8\mu} t = -\frac{x}{h} - \log\left(1 - \frac{x}{h}\right) \quad (42)$$

Table 2 provides a summary of state of the art on capillary rise experiments.

**Table 2.** Summary of state of the art on capillary rise experiments.

Reference	Aim of Research	Experimental Details	Methodology and Notes
Wiel-Shafran et al. (2005, 2006) [37,104]	<ul style="list-style-type: none"> <li>To study the effects of surfactant accumulation due to greywater irrigation by conducting capillary rise experiments.</li> </ul>	<ul style="list-style-type: none"> <li>Capillary rise experiments conducted using 25 cm height, 2.5 cm diameter soil columns.</li> <li>A quarry sand and a native loess from Negev Desert (Israel).</li> <li>A commercial detergent (containing anionic and non-ionic surfactants).</li> <li>LABS-100 (anionic surfactant)</li> <li>Imbentin-UGM/070 (non-ionic surfactant).</li> </ul>	<ul style="list-style-type: none"> <li>Capillary rise equation was derived using Poiseuille's law.</li> <li>Authors found evidence that surfactant accumulation might lead to soil hydrophobicity and formation of water repellent soils.</li> </ul>
Ishiguro and Fujii (2008) [86]	<ul style="list-style-type: none"> <li>"To propose a model for evaluating effects of an anionic surfactant on upward infiltration under saturated conditions in porous materials with highly contrasting wettability" [103].</li> </ul>	<ul style="list-style-type: none"> <li>Capillary rise experiments conducted using 60 cm height and 2 cm diameter soil columns.</li> <li>Five different porous media: hydrophilic (glass beads and sand) and hydrophobic (leaf mold, peat moss, polyethylene particles).</li> <li>Solutions of sodium dodecyl sulfate (SDS) (anionic surfactant) at different concentrations.</li> </ul>	<ul style="list-style-type: none"> <li>By using Darcy's law and Washburn equation, a simplified Green–Ampt-type upward infiltration theory under saturated conditions was introduced.</li> <li>Sharp wetting front was assumed.</li> <li>Surfactant's effects of contact angle and wettability, and influence of adsorption were investigated.</li> <li>Influence of SDS adsorption was mentioned, but results were mainly focused on swelling which is observed in leaf mold.</li> </ul>
McGinnis (2001) and Weisbrod et al. (2009) [73,85]	<ul style="list-style-type: none"> <li>To study if the decrease in surface tension due to high salinity solutions has an impact on imbibition characteristics of dry and prewetted porous media.</li> </ul>	<ul style="list-style-type: none"> <li>Static and dynamic capillary rise experiments conducted using 20 cm height, 4.5 cm diameter soil columns.</li> <li>Four commercial silica sands of 40/50, 30/40, 20/30, and 12/20 grades.</li> <li>Three imbibing solutions: n-hexane, 5 molal NaNO<sub>3</sub>, pure water.</li> </ul>	<ul style="list-style-type: none"> <li>Static method assumes a sharp wetting front in equilibrium with constant saturation in the wetted volume.</li> <li>Dynamic method introduces a modified Green–Ampt model to account for the dynamic and rate-dependent capillary rise process.</li> <li>Static and dynamic methods lead to significant differences in contact angle calculations.</li> </ul>
Liu et al. (2014) [17]	<ul style="list-style-type: none"> <li>To properly account for contact angle of soils by using Lucas–Washburn equation through conducting capillary rise experiments.</li> </ul>	<ul style="list-style-type: none"> <li>Capillary rise experiments conducted using a 44.5-mm height, 5.75-mm diameter soil columns.</li> <li>Two types of porous media: an Ohio subgrade soil and a silica sand.</li> <li>Two imbibing solutions: pentane and pure water.</li> </ul>	<ul style="list-style-type: none"> <li>Authors investigate the Lucas Washburn equation by considering the equation without gravity and inertia (Method 1), considering it without gravity (Method 2), and considering it without inertia (Method 3) while incorporating effects of tortuosity in each method.</li> <li>Authors note that Method 3 provides the best fit.</li> <li>Authors note that two main factors relating contact angle with aggregate size are organic matter content (for Ohio subgrade soil) and roughness (for silica sand).</li> </ul>

## 7. Summary

Various solutes that enter or exist in the subsurface have surface-active properties and their flow and transport is influenced by changes in capillary pressure based on their concentration-dependent effects on the surface tension, density of the liquid, and the contact angle at the solid–liquid interface. These surface-active solutes can alter the geotechnical and hydraulic properties of the vadose zone by changing soil moisture characteristics and unsaturated hydraulic conductivity relations, causing flow perturbations because of induced soil water pressure gradients, and even affecting soil's mechanical properties (e.g., reductions in tensile strength). Although the effects of surface-active



solute accumulation in the subsurface will be increasingly critical in the future due to increasing anthropogenic activities, freshwater scarcity, and climate change, the research on flow, transport, and fate of these solutes in vadose zone is limited. To understand the effects of these solutes on subsurface hydraulic and geotechnical properties, conceptual and numerical models are required to consider the dependence of capillary pressure on concentration-dependent changes in surface tension, density, and contact angle and the dependence of hydraulic conductivity on concentration-dependent changes in kinematic viscosity and moisture content.

Capillary rise is a phenomenon that occurs spontaneously where liquids rush into relatively dry hydrophilic porous media against friction forces and gravity. This spontaneous imbibition is induced by capillary forces which depend on surface tension and the density of the liquid, the contact angle at the solid–liquid interface and the effective pore radius. Capillary rise experiments are primarily used to determine the contact angle and the wetting properties of porous media through indirect procedures to circumvent the need for direct geometric contact angle measurements, which are impossible to perform for complex porous media such as soils. Moreover, surface-active solutes of geo-environmental interest and their effects on soil capillarity can be investigated by using them as imbibing solutions in capillary rise experiments. Investigating the influence of surface-active solutes on the flow and transport of the unsaturated soil zone is a highly complex problem that is dependent on various factors such as solute concentration, solute chemical properties, chemical properties of pore water, properties of the porous media, hydraulic hysteresis, and many other elements (Figure 7). Surface-active solutes' effects on hydraulic and geotechnical properties of the unsaturated porous media may be much more extensive and prevalent than generally assumed. Currently, there is insufficient research on surface-active solute effects in the subsurface and there is a pressing need to expand on a wider range of surface-active solutes in porous media with differing physical and physicochemical properties. Capillary rise experiments can be useful for performing systematic analyses of various surface-active solutes' concentration-dependent effects on capillarity and wettability of different types of porous media with varying properties. This paper presents a literature review on capillary rise experiments on porous media with a focus on how these experiments are being utilized to quantify the influence of surface-active solutes on hydraulic and geotechnical properties in the subsurface.

**Author Contributions:** Conceptualization, S.B. and R.B.; methodology, S.B.; investigation, S.B.; writing—original draft preparation, S.B.; writing—review and editing S.B. and R.B.; visualization, S.B.; supervision, R.B.; funding acquisition, R.B. All authors have read and agreed to the published version of the manuscript.

**Funding:** This research was funded by the Natural Sciences and Engineering Research Council of Canada (NSERC) through the Discovery Grant program to 2nd Author.

**Conflicts of Interest:** The authors declare no conflict of interest.

## References

1. Henry, E.J.; Smith, J.E. Surfactant-Induced Flow Phenomena in the Vadose Zone: A Review of Data and Numerical Modeling. *Vadose Zo. J.* **2003**, *2*, 154–167. [[CrossRef](#)]
2. Karagunduz, A.; Pennell, K.D.; Young, M.H. Influence of a Nonionic Surfactant on the Water Retention Properties of Unsaturated Soils. *Soil Sci. Soc. Am. J.* **2001**, *65*, 1392–1399. [[CrossRef](#)]
3. Karagunduz, A.; Young, M.H.; Pennell, K.D. Influence of Surfactants on Unsaturated Water Flow and Solute Transport. *Water Resour. Res.* **2015**, *51*, 1977–1988. [[CrossRef](#)]
4. Bashir, R.; Smith, J.E.; Stolle, D.F.E. Surfactant Flow and Transport in the Vadose Zone: A Numerical Experiment. *Environ. Geotech.* **2018**, *7*, 361–372. [[CrossRef](#)]
5. Henry, E.J.; Smith, J.E.; Warrick, A.W. Solubility Effects on Surfactant-Induced Unsaturated Flow through Porous Media. *J. Hydrol.* **1999**, *223*, 164–174. [[CrossRef](#)]
6. Bashir, R.; Smith, J.E.; Stolle, D.F. Surfactant-Induced Unsaturated Flow: Instrumented Horizontal Flow Experiment and Hysteretic Modeling. *Soil Sci. Soc. Am. J.* **2008**, *72*, 1510–1519. [[CrossRef](#)]

7. Henry, E.J.; Smith, J.E. The Effect of Surface-Active Solutes on Water Flow and Contaminant Transport in Variably Saturated Porous Media with Capillary Fringe Effects. *J. Contam. Hydrol.* **2002**, *56*, 247–270. [[CrossRef](#)]
8. Smith, J.E.; Henry, E.J.; Bashir, R. Solute-Dependent Capillarity-Induced Focused Flow during Infiltration into Alcohol-Contaminated Soil. *Vadose Zo. J.* **2011**, *10*, 403–411. [[CrossRef](#)]
9. Boduroglu, S.; Bashir, R. Numerical Experiments on Flow and Transport of Various Surfactant Solutions in the Vadose Zone. In Proceedings of the GeoEdmonton, Edmonton, AB, Canada, 23–26 September 2018; The Canadian Geotechnical Society: Edmonton, AB, Canada, 2018.
10. Smith, J.E.; Gillham, R.W. Effects of Solute Concentration-Dependent Surface Tension on Unsaturated Flow: Laboratory Sand Column Experiments. *Water Resour. Res.* **1999**, *35*, 973–982. [[CrossRef](#)]
11. Lu, N.; Likos, W.J. Rate of Capillary Rise in Soil. *J. Geotech. Geoenviron. Eng.* **2004**, *130*, 646–650. [[CrossRef](#)]
12. Soleimani-Fard, H.; König, D.; Goudarzy, M. Experimental and Numerical Analyses of Uprising Moisture in Fine Grained Soils. *J. Geoengin.* **2021**, *16*, 001–014. [[CrossRef](#)]
13. Li, Y.; Zhang, C.; Chen, C.; Chen, H. Calculation of Capillary Rise Height of Soils by SWCC Model. *Adv. Civ. Eng.* **2018**, *2018*, 5190354. [[CrossRef](#)]
14. Heidar Barghi, M. *Use of Capillary Action to Control Soil Moisture*; University of Birmingham: Birmingham, UK, 2018.
15. Letey, J.; Carrillo, M.L.K.; Pang, X.P. Approaches to Characterize the Degree of Water Repellency. *J. Hydrol.* **2000**, *231–232*, 61–65. [[CrossRef](#)]
16. Selker, J.S.; Schroth, M.H. Evaluation of Hydrodynamic Scaling in Porous Media Using Finger Dimensions. *Water Resour. Res.* **1998**, *34*, 1935–1940. [[CrossRef](#)]
17. Liu, Z.; Yu, X.; Wan, L. Capillary Rise Method for the Measurement of the Contact Angle of Soils. *Acta Geotech.* **2014**, *11*, 21–35. [[CrossRef](#)]
18. Ishakoglu, A.; Baytas, A.F. The Influence of Contact Angle on Capillary Pressure–Saturation Relations in a Porous Medium Including Various Liquids. *Int. J. Eng. Sci.* **2005**, *43*, 744–755. [[CrossRef](#)]
19. Tarchitzky, J.; Lerner, O.; Shani, U.; Arye, G.; Lowengart-Aycicegi, A.; Brener, A.; Chen, Y. Water Distribution Pattern in Treated Wastewater Irrigated Soils: Hydrophobicity Effect. *Eur. J. Soil Sci.* **2007**, *58*, 573–588. [[CrossRef](#)]
20. Doerr, S.H.; Shakesby, R.A.; Walsh, R.P.D. Soil Water Repellency: Its Causes, Characteristics and Hydro-Geomorphological Significance. *Earth-Science Rev.* **2000**, *51*, 33–65. [[CrossRef](#)]
21. Maimon, A.; Gross, A.; Arye, G. Greywater-Induced Soil Hydrophobicity. *Chemosphere* **2017**, *184*, 1012–1019. [[CrossRef](#)]
22. Beatty, S.M.; Smith, J.E. Fractional Wettability and Contact Angle Dynamics in Burned Water Repellent Soils. *J. Hydrol.* **2010**, *391*, 97–108. [[CrossRef](#)]
23. Ritsema, C.J.; Dekker, L.W. How Water Moves in a Water Repellent Sandy Soil: 2. Dynamics of Fingered Flow. *Water Resour. Res.* **1994**, *30*, 2519–2531. [[CrossRef](#)]
24. Gross, A.; Mohamed, M.R.; Anda, M.; Ho, G. Effectiveness of Wetting Agents for Irrigating Sandy Soils. *Water* **2011**, *38*, 154–157.
25. König, G.; Reetz, M.T.; Thiel, W. 1-Butanol as a Solvent for Efficient Extraction of Polar Compounds from Aqueous Medium: Theoretical and Practical Aspects. *J. Phys. Chem. B* **2018**, *122*, 6975–6988. [[CrossRef](#)] [[PubMed](#)]
26. Jazwiec, A. *Focused Flow During Water Infiltration into Ethanol Contaminated Unsaturated Porous Media*; McMaster University: Hamilton, ON, Canada, 2018.
27. Vuong, K.H. Modeling the Fate of Groundwater Contaminants Resulting from Leakage of Butanol-Blended Fuel. Master’s Thesis, Department of the Air Force, Air Force Institute of Technology, Air University, Wright-Patterson Air Force Base, Fairborn, OH, USA, 2010.
28. Karimi, K.; Tabatabaei, M.; Sárvári Horváth, I.; Kumar, R. Recent Trends in Acetone, Butanol, and Ethanol (ABE) Production. *Biofuel Res. J.* **2015**, *2*, 301–308. [[CrossRef](#)]
29. Olkowska, E.; Ruman, M.; Polkowska, Ž. Occurrence of Surface Active Agents in the Environment. *J. Anal. Methods Chem.* **2014**, *2014*, 769708. [[CrossRef](#)]
30. Li, Q. *Effect of Surfactants on the Sorption and Transport of Cu (II) in a Sandy Soil: Batch, Column Experiments and Modeling*; Concordia University: Montreal, QC, Canada, 2000.
31. Travis, M.J.; Wiel-Shafran, A.; Weisbrod, N.; Adar, E.; Gross, A. Greywater Reuse for Irrigation: Effect on Soil Properties. *Sci. Total Environ.* **2010**, *408*, 2501–2508. [[CrossRef](#)]
32. Travis, M.J.; Weisbrod, N.; Gross, A. Accumulation of Oil and Grease in Soils Irrigated with Greywater and Their Potential Role in Soil Water Repellency. *Sci. Total Environ.* **2008**, *394*, 68–74. [[CrossRef](#)]
33. Paria, S. Surfactant-Enhanced Remediation of Organic Contaminated Soil and Water. *Adv. Colloid Interface Sci.* **2008**, *138*, 24–58. [[CrossRef](#)]
34. Khandoozi, S.; Sharifi, A.; Riazi, M. Chapter 3 - Enhanced Oil Recovery Using Surfactants. In *Chemical Methods*; Hemmati-Sarapardeh, A., Schaffie, M., Ranjbar, M., Dong, M., Li, Z., Eds.; Enhanced Oil Recovery Series; Gulf Professional Publishing: Oxford, UK, 2022; pp. 95–139, ISBN 978-0-12-821931-7.
35. Gross, A.; Shmueli, O.; Ronen, Z.; Raveh, E. Recycled Vertical Flow Constructed Wetland (RVFCW)—a Novel Method of Recycling Greywater for Irrigation in Small Communities and Households. *Chemosphere* **2007**, *66*, 916–923. [[CrossRef](#)]
36. Ghunmi, L.A.; Zeeman, G.; Fayyad, M.; Van Lier, J.B. Grey Water Treatment Systems: A Review. *Crit. Rev. Environ. Sci. Technol.* **2011**, *41*, 657–698. [[CrossRef](#)]

37. Wiel-Shafran, A.; Ronen, Z.; Weisbrod, N.; Adar, E.; Gross, A. Potential Changes in Soil Properties Following Irrigation with Surfactant-Rich Greywater. *Ecol. Eng.* **2006**, *26*, 348–354. [[CrossRef](#)]
38. Mohamed, R.M.S.R.; Kassim, A.H.M.; Anda, M.; Dallas, S. A Monitoring of Environmental Effects from Household Greywater Reuse for Garden Irrigation. *Environ. Monit. Assess.* **2013**, *185*, 8473–8488. [[CrossRef](#)] [[PubMed](#)]
39. Morel, A.; Diener, S. *Greywater Management in Low and Middle-Income Countries, Review of Different Treatment Systems for Households or Neighbourhoods*; EAWAG: Duebendorf, Switzerland, 2006; ISBN 978-3-906484-37-2.
40. Bajpai, D.; Tyagi, V.K. Laundry Detergents: An Overview. *J. Oleo Sci.* **2007**, *56*, 327–340. [[CrossRef](#)] [[PubMed](#)]
41. Huang, Z. *Fate and Transport of Surfactants in Graywater When Applied to Soil*; Colorado State University: Fort Collins, CO, USA, 2013.
42. Human and Environment Risk Assessment Agency (HERA). Human and Environment Risk Assessment Agency (HERA) Revised Linear Alkylbenzene Sulphonate Report (CAS No. 68411-30-3). *Environ. Risk* **2013**, *101*.
43. Leuther, F.; Schlüter, S.; Wallach, R.; Vogel, H.-J. Structure and Hydraulic Properties in Soils under Long-Term Irrigation with Treated Wastewater. *Geoderma* **2019**, *333*, 90–98. [[CrossRef](#)]
44. Dantas, T.; Santanna, V.; Souza, T.; Lucas, C.; Dantas Neto, A.; Aum, P. Microemulsions and Nanoemulsions Applied to Well Stimulation and Enhanced Oil Recovery (EOR). *Brazilian J. Pet. Gas* **2019**, *12*, 251–265. [[CrossRef](#)]
45. Yang, K.; Zhu, L.; Xing, B. Enhanced Soil Washing of Phenanthrene by Mixed Solutions of TX100 and SDBS. *Environ. Sci. Technol.* **2006**, *40*, 4274–4280. [[CrossRef](#)]
46. Harendra, S.; Vipulanandan, C. Sorption and Transport Studies of Cetyl Trimethylammonium Bromide (CTAB) and Triton X-100 in Clayey Soil. *J. Environ. Sci.* **2013**, *25*, 576–584. [[CrossRef](#)]
47. Park, J.; Vipulanandan, C.; Kim, J.W.; Oh, M.H. Effects of Surfactants and Electrolyte Solutions on the Properties of Soil. *Environ. Geol.* **2006**, *49*, 977–989. [[CrossRef](#)]
48. Befkadu, A.A.; Chen, Q. Surfactant-Enhanced Soil Washing for Removal of Petroleum Hydrocarbons from Contaminated Soils: A Review. *Pedosphere* **2018**, *28*, 383–410. [[CrossRef](#)]
49. Mulligan, C.N.; Yong, R.N.; Gibbs, B.F. Surfactant-Enhanced Remediation of Contaminated Soil: A Review. *Eng. Geol.* **2001**, *60* 371–380. [[CrossRef](#)]
50. Mao, X.; Jiang, R.; Xiao, W.; Yu, J. Use of Surfactants for the Remediation of Contaminated Soils: A Review. *J. Hazard. Mater.* **2015**, *285*, 419–435. [[CrossRef](#)] [[PubMed](#)]
51. Organisation for Economic Co-operation and Development (OECD). *Water Resources Allocation*; OECD Studies on Water; OECD: Paris, France, 2015; ISBN 9789264229624.
52. Mousavi, S.A.; Khodadoost, F. Effects of Detergents on Natural Ecosystems and Wastewater Treatment Processes: A Review. *Environ. Sci. Pollut. Res.* **2019**, *26*, 26439–26448. [[CrossRef](#)] [[PubMed](#)]
53. Ying, G.-G. Fate, Behavior and Effects of Surfactants and Their Degradation Products in the Environment. *Environ. Int.* **2006**, *32*, 417–431. [[CrossRef](#)] [[PubMed](#)]
54. Jindal, P.; Sharma, J.; Bashir, R. Effect of Pore-Water Surface Tension on Tensile Strength of Unsaturated Sand. *Indian Geotech. J.* **2016**, *46*, 276–290. [[CrossRef](#)]
55. Buck, R.C.; Franklin, J.; Berger, U.; Conder, J.M.; Cousins, I.T.; De Voogt, P.; Jensen, A.A.; Kannan, K.; Mabury, S.A.; van Leeuwen, S.P.J. Perfluoroalkyl and Polyfluoroalkyl Substances in the Environment: Terminology, Classification, and Origins. *Integr. Environ. Assess. Manag.* **2011**, *7*, 513–541. [[CrossRef](#)]
56. Bouazza, A. Interaction between PFASs and Geosynthetic Liners: Current Status and the Way Forward. *Geosynth. Int.* **2021**, *28*, 214–223. [[CrossRef](#)]
57. Glüge, J.; Scheringer, M.; Cousins, I.T.; DeWitt, J.C.; Goldenman, G.; Herzke, D.; Lohmann, R.; Ng, C.A.; Trier, X.; Wang, Z. An Overview of the Uses of Per- and Polyfluoroalkyl Substances (PFAS). *Environ. Sci. Process. Impacts* **2020**, *22*, 2345–2373. [[CrossRef](#)]
58. Brusseau, M.L.; Yan, N.; Van Glubt, S.; Wang, Y.; Chen, W.; Lyu, Y.; Dungan, B.; Carroll, K.C.; Holguin, F.O. Comprehensive Retention Model for PFAS Transport in Subsurface Systems. *Water Res.* **2019**, *148*, 41–50. [[CrossRef](#)]
59. Organisation for Economic Cooperation and Development (OECD). *Toward a New Comprehensive Global Database of Per- and Polyfluoroalkyl Substances (PFASs)*; OECD: Paris, France, 2018; Volume 39.
60. Brendel, S.; Fetter, É.; Staude, C.; Vierke, L.; Biegel-Engler, A. Short-Chain Perfluoroalkyl Acids: Environmental Concerns and a Regulatory Strategy under REACH. *Environ. Sci. Eur.* **2018**, *30*, 1–11. [[CrossRef](#)]
61. United States Environmental Protection Agency (EPA). *PFAS Strategic Roadmap: EPA's Commitments to Action (2021–2024)* EPA-100-K-21-002; EPA: Washington, DC, USA, 2021; Volume 26.
62. United States Department of Health and Human Services Agency. *United States Department of Health and Human Services Agency for Toxic Substances and Disease Registry Toxicological Profile for Perfluoroalkyls CS274127-A*; United States Department of Health and Human Services Agency: Washington, DC, USA, 2021; Volume 676.
63. Stahl, T.; Heyn, J.; Thiele, H.; Hütther, J.; Failing, K.; Georgii, S.; Brunn, H. Carryover of Perfluorooctanoic Acid (PFOA) and Perfluorooctane Sulfonate (PFOS) from Soil to Plants. *Arch. Environ. Contam. Toxicol.* **2009**, *57*, 289–298. [[CrossRef](#)] [[PubMed](#)]
64. Death, C.; Bell, C.; Champness, D.; Milne, C.; Reichman, S.; Hagen, T. Per- and Polyfluoroalkyl Substances (PFAS) in Livestock and Game Species: A Review. *Sci. Total Environ.* **2021**, *774*, 144795. [[CrossRef](#)] [[PubMed](#)]

65. Kim, Y.R.; White, N.; Bräunig, J.; Vijayasathay, S.; Mueller, J.F.; Knox, C.L.; Harden, F.A.; Pacella, R.; Toms, L.-M.L. Per- and Poly-Fluoroalkyl Substances (PFASs) in Follicular Fluid from Women Experiencing Infertility in Australia. *Environ. Res.* **2020**, *190*, 109963. [CrossRef] [PubMed]
66. The White House Briefing Room Fact Sheet: Biden-Harris Administration Combatting PFAS Pollution to Safeguard Clean Drinking Water for All Americans. Available online: <https://www.whitehouse.gov/briefing-room/statements-releases/2022/06/15/fact-sheet-biden-harris-administration-combatting-pfas-pollution-to-safeguard-clean-drinking-water-for-all-americans/> (accessed on 1 August 2022).
67. Kislik, V.S. Advances in Development of Solvents for Liquid–Liquid Extraction. In *Solvent Extraction: Classical and Novel Approaches*; Elsevier: Oxford, UK, 2012; pp. 451–481, ISBN 978-0-444-53778-2.
68. Pomeau, Y.; Villermaux, E. Two Hundred Years of Capillarity Research. *Phys. Today* **2006**, *59*, 39–44. [CrossRef]
69. Jurin, J., II. An Account of Some Experiments Shown before the Royal Society; with an Enquiry into the Cause of the Ascent and Suspension of Water in Capillary Tubes. *Philos. Trans. R. Soc. London* **1719**, *30*, 739–747. [CrossRef]
70. Laplace, P.S. *Traité de Mécanique Céleste*; A Paris: De L’Imprimerie de Crapelet: Paris, France, 1805; pp. 1–2.
71. Young, T., III. An Essay on the Cohesion of Fluids. *Philos. Trans. R. Soc. London* **1805**, *95*, 65–87. [CrossRef]
72. Selker, J.S.; Keller, C.K.; McCord, J.T. *Vadose Zone Processes*; CRC Press, LLC.: Boca Raton, FL, USA, 1999; pp. 22–56, 111–117. ISBN 9780873719537.
73. McGinnis, T.L. *Determining Contact Angle of Solutions with Varying Surface Tension on Dry and Pre-Wetted Sands*; Oregon State University: Corvallis, OR, USA, 2001.
74. Bashir, R.; Smith, J.E.; Stolle, D.E. The Effect of Ionic Strength on Surfactant-Induced Unsaturated Flow. *Can. Geotech. J.* **2011**, *48*, 644–654. [CrossRef]
75. Allred, B.; Brown, G.O. Surfactant-Induced Reductions of Saturated Hydraulic Conductivity and Unsaturated Diffusivity. In *Surfactant-Enhanced Subsurface Remediation*; ACS Symposium Series; American Chemical Society: Washington, DC, USA, 1995; Volume 594, pp. 16–216, ISBN 9780841232259.
76. Tumeo, M.A. A Survey of the Causes of Surfactant-Induced Changes in Hydraulic Conductivity. *Groundw. Monit. Remediat.* **1997**, *17*, 138–144. [CrossRef]
77. Pham, H.Q.; Fredlund, D.G.; Barbour, S.L. A Study of Hysteresis Models for Soil-Water Characteristic Curves. *Can. Geotech. J.* **2005**, *42*, 1548–1568. [CrossRef]
78. Bashir, R.; Sharma, J.; Stefaniak, H. Effect of Hysteresis of Soil-Water Characteristic Curves on Infiltration under Different Climatic Conditions. *Can. Geotech. J.* **2016**, *53*, 273–284. [CrossRef]
79. Klausner, Y. Fundamentals of Continuum Mechanics of Soils. In *Fundamentals of Continuum Mechanics of Soils*; Springer: London, UK, 1991; p. 209, ISBN 978-1-4471-1679-0.
80. Haines, W.B. Studies in the Physical Properties of Soil. V. The Hysteresis Effect in Capillary Properties, and the Modes of Moisture Distribution Associated Therewith. *J. Agric. Sci.* **1930**, *20*, 97–116. [CrossRef]
81. Bashir, R. *Quantification of Surfactant-Induced Unsaturated Flow in the Vadose Zone*; McMaster University: Hamilton, ON, Canada, 2007.
82. Yan, G.; Li, Z.; Galindo Torres, S.A.; Scheuermann, A.; Li, L. Transient Two-Phase Flow in Porous Media: A Literature Review and Engineering Application in Geotechnics. *Geotechnics* **2022**, *2*, 32–90. [CrossRef]
83. Bashir, R.; Smith, J.E.; Henry, E.J.; Stolle, D. On the Importance of Hysteresis in Numerical Modeling of Surfactant-Induced Unsaturated Flow. *Soil Sediment Contam.* **2009**, *18*, 264–283. [CrossRef]
84. Russo, D.; Jury, W.A.; Butters, G.L. Numerical Analysis of Solute Transport during Transient Irrigation: 1. The Effect of Hysteresis and Profile Heterogeneity. *Water Resour. Res.* **1989**, *25*, 2109–2118. [CrossRef]
85. Weisbrod, N.; McGinnis, T.; Rockhold, M.L.; Niemet, M.R.; Selker, J.S. Effective Darcy-Scale Contact Angles in Porous Media Imbibing Solutions of Various Surface Tensions. *Water Resour. Res.* **2009**, *45*, W00D39. [CrossRef]
86. Ishiguro, M.; Fujii, T. Upward Infiltration into Porous Media as Affected by Wettability and Anionic Surfactants. *Soil Sci. Soc. Am. J.* **2008**, *72*, 741–749. [CrossRef]
87. Wallach, R.; Margolis, M.; Graber, E.R. The Role of Contact Angle on Unstable Flow Formation during Infiltration and Drainage in Wettable Porous Media. *Water Resour. Res.* **2013**, *49*, 6508–6521. [CrossRef]
88. Butt, H.-J.; Graf, K.; Kappl, M. Section 7: Contact Angle Phenomena and Wetting. In *Physics and Chemistry of Interfaces*; Wiley-VCH Verlag GmbH & Co. KGaA: Weinheim, Germany, 2003; pp. 126–129, ISBN 3-527-40413-9.
89. Liu, Q.; Yasufuku, N.; Miao, J.; Ren, J. An Approach for Quick Estimation of Maximum Height of Capillary Rise. *Soils Found.* **2014**, *54*, 1241–1245. [CrossRef]
90. Al-Yaqout, A.F.; Hamoda, M.F. Evaluation of Landfill Leachate in Arid Climate—A Case Study. *Environ. Int.* **2003**, *29*, 593–600. [CrossRef]
91. Faybishenko, B.A. Hydraulic Behavior of Quasi-Saturated Soils in the Presence of Entrapped Air: Laboratory Experiments. *Water Resour. Res.* **1995**, *31*, 2421–2435. [CrossRef]
92. Hird, R.; Bolton, M.D. Clarification of Capillary Rise in Dry Sand. *Eng. Geol.* **2017**, *230*, 77–83. [CrossRef]
93. Lane, K.S.; Washburn, S.E. Capillarity Tests by Capillarimeter and by Soil Filled Tubes. In Proceedings of the Twenty-Sixth Annual Meeting of the Highway Research Board, Washington, DC, USA, 5–8 December 1946; Volume 26, pp. 460–473.
94. Peck, R.B.; Hanson, W.E.; Thornburn, T.H. *Foundation Engineering*; Wiley: New York, NY, USA, 1974; ISBN 0471675857.



95. Kumar, S.; Malik, R.S. Verification of Quick Capillary Rise Approach for Determining Pore Geometrical Characteristics in Soils of Varying Texture. *Soil Sci.* **1990**, *150*, 883–888. [[CrossRef](#)]
96. Letey, J.; Osborn, J.; Pelishek, R.E. Measurement of Liquid-Solid Contact Angles in Soil and Sand. *Soil Sci.* **1962**, *93*, 149–153. [[CrossRef](#)]
97. Myers, D. *Surfaces, Interfaces, and Colloids: Principles and Applications*, 2nd ed.; John Wiley & Sons, Inc.: Hoboken, NJ, USA, 1999; ISBN 0-471-23499-0.
98. Blake, T.D. The Physics of Moving Wetting Lines. *J. Colloid Interface Sci.* **2006**, *299*, 1–13. [[CrossRef](#)]
99. Rapp, B.E. Fluid Surface Effects. In *Microfluidics: Modeling, Mechanics and Mathematics*; Elsevier: Oxford, UK, 2017; pp. 419–443.
100. Washburn, E.W. The Dynamics of Capillary Flow. *Phys. Rev.* **1921**, *17*, 273–283. [[CrossRef](#)]
101. Heber Green, W.; Ampt, G.A. Studies on Soil Physics. *J. Agric. Sci.* **1911**, *4*, 1. [[CrossRef](#)]
102. McBride, J.F.; Simmons, C.S.; Cary, J.W. Interfacial Spreading Effects on One-Dimensional Organic Liquid Imbibition in Water-Wetted Porous Media. *J. Contam. Hydrol.* **1992**, *11*, 1–25. [[CrossRef](#)]
103. Brooks, R.H.; Corey, A.T. Hydraulic Properties of Porous Media. *Hydrol. Pap.* **1964**, *3*, 27.
104. Shafran, A.W.; Gross, A.; Ronen, Z.; Weisbrod, N.; Adar, E. Effects of Surfactants Originating from Reuse of Greywater on Capillary Rise in the Soil. *Water Sci. Technol.* **2005**, *52*, 157–166. [[CrossRef](#)]
105. George, A.L.; White, G.F. Optimization of the Methylene Blue Assay for Anionic Surfactants Added to Estuarine and Marine Water. *Environ. Toxicol. Chem.* **2009**, *18*, 2232–2236. [[CrossRef](#)] [[PubMed](#)]
106. Malik, R.S.; Laroussi, C.H.; de Backer, I.W. Penetration Coefficient in Porous Media. *Soil Sci.* **1981**, *132*, 394–401. [[CrossRef](#)]
107. Marmur, A. Kinetics of Penetration into Uniform Porous Media: Testing the Equivalent-Capillary Concept. *Langmuir* **2003**, *19*, 5956–5959. [[CrossRef](#)]